BIOCHEMISTRY
including biophysical chemistry & molecular biology
Article

Biochemistry **2010,** *49,* 8729–8738 8729
DOI: 10.1021/bi100572j

The H187R Mutation of the Human Prion Protein Induces Conversion of Recombinant Prion Protein to the PrP^{Sc}-like Form[†]

Laszlo L. P. Hosszu,[‡,§] M. Howard Tattum,[‡] Samantha Jones,[‡] Clare R. Trevitt,[‡,§] Mark A. Wells,[§] Jonathan P. Waltho,[§] John Collinge,[‡] Graham S. Jackson,[‡] and Anthony R. Clarke*[,‡]

[‡]*MRC Prion Unit, UCL Department of Neurodegenerative Disease, Institute of Neurology, Queen Square, London WC1N 3BG, U.K., and* [§]*Krebs Institute for Biomolecular Research, Department of Molecular Biology and Biotechnology, Firth Court, Western Bank, University of Sheffield, Sheffield S10 2TN, U.K.*

Received April 14, 2010; Revised Manuscript Received August 4, 2010

ABSTRACT: Prion diseases are associated with a conformational switch in the prion protein (PrP) from its normal cellular form (denoted PrP^{C}) to a disease-associated "scrapie" form (PrP^{Sc}). A number of PrP^{Sc}-like conformations can be generated by incubating recombinant PrP^{C} at low pH, indicating that protonation of key residues is likely to destabilize PrP^{C}, facilitating its conversion to PrP^{Sc}. Here, we examine the stability of human PrP^{C} with pH and find that PrP^{C} fold stability is significantly reduced by the protonation of two histidine residues, His187 and His155. Mutation of His187 to an arginine, which imposes a permanently positively charged residue in this region of the protein, has a dramatic effect on the folding of PrP^{C}, resulting in a molecule that displays a markedly increased propensity to oligomerize. The oligomeric form is characterized by an increased β-sheet content, loss of fixed side chain interactions, and partial proteinase resistance. Hence, the protonation state of H187 appears to be crucial in determining the conformation of PrP; the unprotonated form favors native PrP^{C}, while the protonated form favors PrP^{Sc}-like conformations. These results are relevant to the pathogenic H187R mutation found in humans, which is associated with an inherited prion disease [also termed Gerstmann-Sträussler-Scheinker (GSS) syndrome] with unusual features such as childhood neuropsychiatric illness. Our data imply that the intrinsic instability of the PrP^{C} conformation in this variant is caused by a positive charge at this site in the protein. This mutation is distinct from all those associated with GSS, which have much more subtle physical consequences. The degree of instability might be the cause of the unusually early onset of mental disturbance in affected individuals.

Prion diseases, such as bovine spongiform encephalopathy (BSE) in cattle and Creutzfeldt-Jakob disease (CJD), kuru, and Gerstmann-Sträussler-Scheinker (GSS) syndrome in humans, are similar to other neurodegenerative diseases, such as Alzheimer's and Parkinson's, in that they are characterized by the accumulation of a misfolded form of a normal host-encoded protein, in this case prion protein (PrP)[1] (*1*, *2*). They are, however, distinct as they produce infectious material. PrP is typically deposited in amyloid plaques within the brain, and the disease process is characterized by neuronal cell loss, vacuolation of brain tissue, cognitive loss, motor deficits, and ultimately death (*2*). The infectious agent appears to be composed solely or primarily of a misfolded form of PrP (*3*, *4*). This disease-associated or "scrapie" form of the protein (PrP^{Sc}) is characterized by its detergent insolubility, its aggregation state, and a dramatic increase in protease resistance and β-sheet content when compared to those of its normal cellular form (PrP^{C}) (*5*). No consistent post-translational or covalent differences between these two forms have been determined, and it is believed that they are distinguished solely by the altered conformation and aggregation state. The most coherent and general model for the formation of PrP^{Sc} is that the prion protein fluctuates between its dominant native PrP^{C} state and a series of minor conformations (*6*, *7*), one or a set of which can self-associate in an ordered manner to form a stable supramolecular PrP^{Sc} structure that is composed of PrP monomers. PrP^{Sc} can then be stabilized by complementary association with like molecules or can actively convert PrP molecules into a like conformation (*2*).

The fact that PrP^{Sc} has never been purified to homogeneity and characterized rigorously has led to considerable uncertainty about the precise nature of the infectious unit and also to speculation regarding the requirement for cofactors. Nonetheless, the central role of PrP in the disease process is demonstrated by the observation that inherited mutations within the PrP gene *PRNP* may lead to prion disease with production of transmissible prions. More than 30 of these *PRNP* mutations have been identified, the majority of which lead to the production of transmissible agents (*2*, *8*). Interestingly, these mutant forms when expressed as recombinant proteins and analyzed in their purified state do not obviously destabilize the normal cellular form of the protein; hence, PrP^{C} instability does not appear to be the major factor in predisposing it to convert to PrP^{Sc} (*9*).

Given that a defining event in prion disease pathology is the conformational change of PrP^{C} to PrP^{Sc}, much effort has been

[†]This work was funded by the UK Medical Research Council.

*To whom correspondence should be addressed. Telephone: +44 (0)207 837 4888. Fax: +44 (0)207 676 2180. E-mail: a.r.clarke@prion.ucl.ac.uk.

[1]Abbreviations: AUC, analytical ultracentrifugation; CD, circular dichroism; DTNB, 5,5′-dithiobis(2-nitrobenzoic acid); DTT, 1,4-dithiothreitol; PrP, prion protein; PrP^{C}, cellular PrP isoform; PrP^{Sc}, pathogenic (scrapie) PrP isoform; PrP^{91-231}, human prion protein (residues 91−231); EDTA, ethylenediaminetetraacetic acid; FTIR, Fourier transform infrared spectroscopy; GuHCl, guanidine hydrochloride; HSQC, heteronuclear single-quantum coherence; SDS−PAGE, sodium dodecyl sulfate−polyacrylamide gel electrophoresis; TSP, sodium 3-trimethylsilyl [2,2,3,3-$^{2}H_4$]propionate; 2D, two-dimensional; 3D, three-dimensional.

Published on Web 08/18/2010

devoted to characterizing the structural and dynamic behavior of both the cellular and pathogenic forms of prion protein, and factors that may affect the conversion process. A number of studies have shown that destabilizing PrP by lowering the pH and/or chemical denaturants favors the formation of alternatively folded intermediates (*10*−*14*). These conditions are relevant as there is considerable evidence that endosome-like organelles or lysosomes, with their locally acidic environments, are plausible locations for PrP^{Sc} propagation (*15*). A number of these intermediates display some if not all of the characteristics of PrP^{Sc}, such as increased β-sheet content, protease resistance, and a propensity for oligomerization, and some have been associated with infectivity (*16*−*19*).

Acidic conditions can result in the protonation of histidine, glutamate, aspartate, lysine, and arginine residues, and a number of molecular dynamics (MD) simulations have indicated that protonation of side chain groups results in increased conformational mobility and β-sheet content within PrP^{C} (*20*, *21*). Comparison of the solution structure of recombinant human PrP^{C} ($huPrP^{C}$) at pH 7.0 with that at pH 4.5 supports this, with local conformational differences and fraying of helices being observed (*22*). Further studies also show that at lower pH (3.5) the C-terminal region of helix II of mouse PrP is significantly more mobile and disordered (*23*). Thus, both experimental and computational studies suggest that acidic pH, and hence the protonation of pivotal residues, may be important in the conformational switch between PrP^{C} and PrP^{Sc}.

Here, we show that the structural stability of the recombinantly expressed cellular form of human prion protein, here termed α-PrP, is strongly dependent on the protonation state of two residues, with apparent pK_a values of approximately 6.3, the deprotonated protein being more stable. The pK_a values are consistent with protonation of histidine residues. We find that the regions of the protein that experience the largest changes in NMR chemical shift are associated with histidine 187, and to a lesser extent histidine 155. Mutation of histidine 187 to an arginine, thus imposing a permanently protonated positively charged residue at this position, results in a protein that is markedly destabilized, which readily aggregates to form β-sheet multimers. This study suggests that this region of the protein is instrumental in the conversion of PrP^{C} to PrP^{Sc}, a conclusion that is supported by a number of disease-causing mutations that introduce positive charge into this region of the protein (*8*, *24*−*27*).

EXPERIMENTAL PROCEDURES

Preparation of Wild-Type and H187R Mutant Recombinant PrP Proteins. The protein construct used in this study comprised residues 91−231 of the human prion protein (PrP^{91-231}). The open reading frame of the human PrP gene (*PRNP*), containing methionine at residue 129, was amplified by polymerase chain reaction (PCR) using oligonucleotide primers designed to create a unique N-terminal *Bam*HI site and C-terminal *Hin*dIII site for directional cloning of the fragment into expression vector pTrcHisB (Invitrogen Corp.). The primer corresponding to the N-terminal region of *PRNP* to be expressed was designed to mutate a glycine at codon 90 to methionine and to incorporate a thrombin cleavage site, with the C-terminal primer replacing a methionine residue at position 232 with a stop codon. Standard protocols for site-directed mutagenesis were used to create the H187R mutation; its presence was confirmed by DNA sequencing.

Wild-type and H187R mutant PrPs were expressed in *Escherichia coli* host strain BL21(DE3) (Novagen) and grown in LB medium containing 100 μg/mL carbenicillin at 37 °C to an OD_{600} of 0.6. Expression was then induced by the addition of isopropyl β-D-galactopyranoside (IPTG) to a final concentration of 1 mM. Following induced growth for 4 h, the cells were harvested by centrifugation at 8500 rpm for 10 min. The protein were expressed in inclusion bodies. Cell pellets were resolubilized in 6 M GuHCl and 50 mM Tris-HCl (pH 8.0), purified initially on a Ni-NTA-Sepharose (Quiagen) column pre-equilibrated with the same buffer, and then oxidized in the unfolded state (*7*).

Wild-type protein was refolded by dialysis into 10 mM Tris-HCl and 10 mM sodium acetate (pH 8) and further purified on the Ni-NTA-Sepharose column in the native state. The H187R mutant protein was insoluble at neutral or near-neutral pHs and was refolded from 6 M GuHCl (pH 8.0) by dialysis against 10 mM sodium acetate and 0.02% (w/v) sodium azide (pH 3.5). Following refolding, precipitated material was removed by centrifugation at 150000*g* for 4 h. Wild-type protein in the β conformation (β-PrP) was produced as previously described (*14*). Briefly, purified α-PrP was denatured in 6 M GuHCl in the presence of 100 mM DTT, refolded under reducing conditions by dialysis against 10 mM sodium acetate and 2 mM DTT (pH 4.0), and subjected to ultracentrifugation at 150000*g* for 4 h. The proteins were estimated to be >95% pure by SDS−PAGE.

Expression and purification of ^{15}N-labeled wild-type PrP^{91-231} for NMR were conducted as described previously (*28*). Samples were stored in 6 M GuHCl and 100 mM EDTA (pH 8.0) at −20 °C, prior to use. Protein samples were dialyzed into 20 mM sodium acetate-d_3 and 0.02% (w/v) sodium azide (pH 5.5) and then concentrated in Amicon50 pressure cells; 10% D_2O (v/v) and 1 mM TSP were added to the NMR samples to provide NMR reference signals.

Circular Dichroism Spectroscopy. Circular dichroism spectra were recorded with a Jasco J-715 spectropolarimeter at 20 °C. The sample temperature was controlled with a circulating water bath. Far-UV (amide) CD spectra were recorded between 190 and 250 nm using a 0.01 cm path length quartz cuvette. The scanning speed was 100 nm/min with a data pitch of 1 nm, a bandwidth of 2 nm, and a response time of 4 s. The protein concentrations and sample buffer conditions were as follows: 1.15 mg/mL solution 10 mM sodium acetate (pH 3.5) for H187R; 0.5 mg/mL solution of 10 mM Tris and 10 mM sodium acetate (pH 8.0) for α-PrP, and 1.3 mg/mL solution of 10 mM sodium acetate and 2 mM DTT (pH 4.0) for β-PrP. All samples contained 0.02% (w/v) sodium azide. Ten spectra were averaged. Near-UV (aromatic) CD spectra were recorded between 250 and 310 nm in an identical manner using the same protein samples, except a 1 cm path length quartz cuvette was used. The sample used for the near-UV spectra of denatured α-PrP was a 0.4 mg/mL solution in 6 M GuHCl, 10 mM Tris, and 10 mM sodium acetate (pH 8.0).

Equilibrium Unfolding Experiments. For the equilibrium unfolding experiments, the amide CD absorption of wild-type PrP^{91-231} at 10 μM was recorded at varying concentrations of GuHCl at various pHs (*7*, *29*) in 10 mM Tris and 10 mM sodium acetate (pH 8.0). The ellipticity signal (α) was converted to the proportion of molecules in the native state (α_N) according to the relationship $\alpha_N = (\theta - \theta_U)/(\theta_N - \theta_U)$, where θ_U and θ_N are the ellipticity signals for the unfolded and native states, respectively. Data were fitted to the following function:

$$\alpha_N = [K_{N/U} \times \exp(mD)]/(1 + K_{N/U}) \quad (1)$$

where m represents the sensitivity of the unfolding transition to denaturant, $K_{N/U}$ is the equilibrium constant between the native

and unfolded states at a particular denaturant activity, and D is the denaturant activity (see below).

Equation 1 assumes a linear dependence of the free energy change of protein folding (ΔG) on the concentration of denaturant. However, this relationship is known to be nonlinear, particularly at high concentrations of denaturant (*30*). To allow more accurate extrapolation of data to calculate folding parameters in the absence of denaturant, it is useful to linearize the scale by converting denaturant concentration ([GuHCl]) to molar denaturant activity (D), according to the relationship

$$D = C_{0.5}[\mathrm{GuHCl}]/(C_{0.5} + [\mathrm{GuHCl}]) \quad (2)$$

where $C_{0.5}$ is an empirically derived denaturation constant, which is specific to each denaturant and varies with temperature. For example, for GuHCl at 20 °C (the temperature used for the equilibrium denaturation experiments), $C_{0.5}$ = 7.5 M (*31*).

The equilibrium constant for folding in water was plotted as a function of pH, and the data were fitted to a modification of the van't Hoff isochore (*32*). The data were fitted to empirical functions describing one, two, and three independent pK_a values. An equation containing two independent pK_a values was the only one that could describe the data accurately, and in Figure 1, data are fitted to the following function:

$$a = a\log(\mathrm{p}K_1 - \mathrm{pH})$$

$$b = a\log(\mathrm{p}K_2 - \mathrm{pH})$$

$$(K_0 + aK_1 + bK_2 + abK_1K_2/K_0)/(1 + a + b + ab) \quad (3)$$

A 10 mM Tris/10 mM sodium acetate buffer mix was used for the equilibrium unfolding at varying pHs.

NMR Spectroscopy. NMR spectra were recorded at 298 K (25 °C) on a Bruker DRX-600 spectrometer equipped with a 5 mm ^{13}C, ^{15}N, ^{1}H triple-resonance probe. Proton chemical shifts were referenced to 1 mM TSP added to the samples. ^{15}N chemical shifts were calculated relative to TSP, using the gyromagnetic ratios of ^{15}N and ^{1}H (^{15}N/^{1}H = 0.101329118). NMR data were processed and analyzed on Linux Workstations using Felix 2004 (Accelrys, San Diego, CA). For the pH titration, a 1.1 mM sample of ^{15}N-labeled PrP$^{91-231}$ was titrated with aliquots of 0.1 M HCl, to a final pH of 3.85. Following each addition, the sample was allowed to equilibrate for 60 min at 298 K, before being placed in the magnet. One-dimensional (1D) ^{1}H and 2D ^{1}H−^{15}N HSQC spectra were acquired at the same temperature. ^{1}H−^{15}N HSQC spectra were acquired using sensitivity-enhanced pulsed field gradient coherence selection (*33*, *34*) with acquisition times of 138 and 87.5 ms in the ^{1}H and ^{15}N dimensions, respectively. The intensities of resolved HSQC resonances were measured and normalized to the intensity of the backbone resonance of residue A117, whose intensity remained approximately constant throughout the titration.

Determination of Sample Solubility. For determination of pH solubility, 10 μL of protein in 10 mM sodium acetate and 0.02% (w/v) sodium azide (pH 3.0) was rapidly mixed into 990 μL of 10 mM sodium citrate and 10 mM citric acid (varying pHs) and then centrifuged for 5 min at 13200 rpm (16200*g*) in an Eppendorf microfuge. The protein absorbance at 280 nm was measured and the protein concentration determined using an extinction coefficient of 19893 M^{-1} cm^{-1}. The initial protein concentrations were as follows: 142 μM (2.34 mg/mL) H187R, 114 μM (1.89 mg/mL) α-PrP, and 97 μM (1.6 mg/mL) β-PrP.

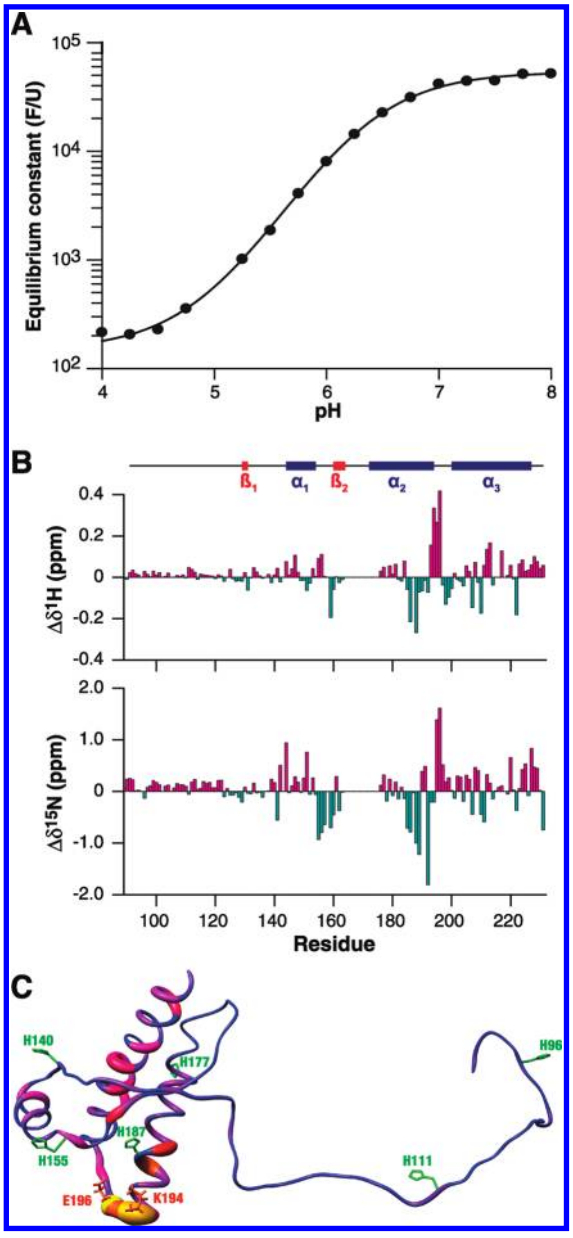

FIGURE 1: Effect of pH on the structure and stability of wild-type α-PrP. (A) Effect of pH on the free energy of folding of wild-type PrP. The equilibrium unfolding of PrP at various pHs in the presence of GuHCl was monitored by far-UV circular dichroism, and the data were fitted to a nonlinear least-squares two-state model with pre- and post-transition baseline slopes (see Experimental Procedures). Two pK_a values control the pH dependence of PrP unfolding, with apparent values of 6.2 and 6.4, suggestive of the involvement of histidine residues. (B) Chemical shift changes in the prion protein native state caused by acidification. ^{1}H and ^{15}N chemical shift changes ($\Delta\delta$) observed in α-PrP upon reduction of the pH from 5.5 to 3.85. Secondary structure elements of the α-PrP native state are represented by bars at the top of the figure. (C) Chemical shift changes in the wild-type prion protein native state caused by acidification. ^{1}H and ^{15}N chemical shift changes ($\Delta\delta$) observed in α-PrP upon reduction of pH from 5.5 to 3.85, displayed on the three-dimensional structure of PrP^{C} (*28*), by a color scale, ranging from blue to red to yellow, and also radii of the backbone, with the magnitude of shift changes increasing from a thin blue ribbon to a wide yellow ribbon. The location of histidine residues, K194, and E196 are shown with their side chains in ball-and-stick representation. The regions of greatest chemical shift change are centered around histidines 155 and 187, in particular within the loop linking helices II and III, which forms the interface in a domain-swapped form of prion protein (*50*). This figure was prepared using UCSF Chimera (*67*).

Analysis of the Sulfhydryl State. The status of the disulfide bond in H187R PrP was determined by measuring the amount of reduced cysteines with the Ellman test (*35*). Briefly, 33.75 μM H187R was denatured in 6 M GuHCl and 10 mM sodium acetate (pH 8) and mixed with 5 mM DTNB to a final DTNB concentration of 500 μM, and the absorbance at 412 nm measured after incubation for 5 and 15 min at room temperature. Reference samples, consisting of buffer without protein, and buffer containing 33.75 μM DTT were measured in a similar manner. Three independent measurements were taken. The concentration of free sulfhydryl groups was calculated from the following equation:

$$\text{concentration of Sulfhydryl groups} = [A_{412}(\text{sample}) - A_{412}(\text{reference})]/13650 \quad (4)$$

Determination of Protease Resistance. H187R and α-PrP prepared in 10 mM sodium acetate (pH 3.5) at concentrations of 1 mg/mL were digested in the presence of varying concentrations of proteinase K (British Drug Houses) at 37 °C for 1 h. Digestion was terminated by addition of 5 mM AEBSF (Melford Laboratories). Samples were heated to 100 °C for 5 min in SDS loading buffer before electrophoresis on 16% SDS−polyacrylamide gels. Gels were stained with Coomassie blue.

Sedimentation Velocity Analytical Ultracentrifugation (*AUC*). Sedimentation velocity AUC experiments were conducted using a Beckman Optima XL-1 analytical ultracentrifuge at 20 °C. H187R was prepared at 0.09, 0.4, and 0.9 mg/mL in 10 mM sodium acetate (pH 3.5), α-PrP at ~0.8 mg/mL in 10 mM sodium acetate 10 mM Tris (pH 8), and β-PrP at 0.3 and 0.8 mg/mL in 10 mM sodium acetate and 2 mM DTT (pH 4). Samples were loaded into Beckman AUC sample cells with 12 mm optical path two-channel Epon centerpieces, with the matched buffer in the reference sector. Cells were loaded into a AnTi-50 rotor and spun at 50000 rpm; interference scans were acquired immediately on reaching speed and thereafter at 5 min intervals over a period of 16 h. Sedimentation velocity data were analyzed using SEDFIT (version 11.3) (*36*). SEDNTERP (*37*) was used to calculate partial specific volumes of the wild-type and mutant PrPs, and also buffer densities and viscosities, for use in data fitting. The *c*(*s*) distribution fit in SEDFIT (*36*) was used to characterize the sedimentation coefficient distribution of all species present in solution. Frictional ratios were optimized for each data set. Reported sedimentation coefficients are corrected from the experimental values to 20 °C and water [S_w(20,w)] for comparison of samples in different buffer systems. Peak integration was used to determine the proportion of the total sample sedimenting as a discrete species.

Fourier Transform Infrared Spectroscopy. Hydrated film samples were analyzed on an ATR Nicolet Avatar 360 spectrometer with a ZnSe "multibounce" ATR accessory. Protein spectra were compiled from 1024 scans at 4 cm^{-1} resolution and were processed as a ratio of the reference spectra from the bare plate. Samples of α-PrP, β-PrP, and fibrils were deposited on the spectrometer plate at concentrations of 0.1 and 0.01 mg/mL in 5 μL drops. The solutions were air-dried before data were collected.

Thioflavin T Amyloid Binding Assay. For thioflavin T amyloid binding assays, H187R PrP and α-PrP were diluted to 10 and 20 μM in 200 μL of 20 mM sodium acetate (pH 6.0) containing 10 μM thioflavin T on a black 96-well microtiter plate (Greiner Bio-One). Fluorescence was measured (λ_{ex} = 450 nm; λ_{em} = 482 nm) on a Tecan Infinite M1000 microplate reader (N = 4, and significance was calculated with an unpaired t test).

RESULTS

Dependence of Stability on pH; Estimation of pK_a Values in the Unfolded State. We determined the pH sensitivity of wild type α-PrP by performing a series of guanidinium chloride (GuHCl) denaturation experiments at 17 pH values between 4.0 and 8.0 monitored by circular dichroism. The derived equilibrium constants for folding were plotted versus pH (Figure 1A) and show a decrease in the stability of PrP with a decrease in pH. This relationship is controlled by two pK_a values with almost the same value (apparent values of 6.2 and 6.4; the unfolding data did not fit well to the protonation of a single residue). In this regard, it is important to note that the stability of the protein, and hence the derived pK_a values, are sensitive to ionization within the unfolded state. The apparent pK_a values determined here are near the intrinsic pK_a value (≈ 6.6) of histidine, pointing to the protonation of two histidine residues being the likely cause of the decrease in the stability of PrP with a decrease in pH. At the acidic limit of the measurements, where both groups are protonated in the unfolded state, the equilibrium constant ($K_{F/U}$) is approximately 150, and at the basic limit, where they are unprotonated, it is approximately 70000. The pK_a values in the folded state and the stability of the singly protonated species are not uniquely defined by these data.

pH-Induced Perturbation of the PrP Native State. The solution structures of the prion protein from a number of different species (*38*) show that α-PrP consists of a flexibly disordered N-terminal region (residues 23−120) and a structured, predominantly α-helical C-terminal domain (residues 121−231). The latter comprises three α-helices, residues 144−154, 172−194, and 200−227, and a short antiparallel β-sheet spanning residues 129−131 and 161−164. The four histidines in the structured region of α-PrP, H140, H155, H177, and H187, are solvent-exposed to varying degrees and thus likely to have different pK_a values. To determine the extent to which each of these is involved in the destabilization of the protein, the chemical shift changes for backbone amide groups of α-PrP were determined over the pH range from 5.5 to 3.9 using 2D $^1H-^{15}N$ HSQC NMR spectra. In this way, pH-induced changes in conformation could be mapped onto the tertiary structure. The pH range was chosen as human α-PrP exhibits a conformational change between pH 5.5 and 4.4 (*39*), and a number of PrP folding intermediates are formed within this pH range (pH 5.5−4.0) (*10*−*12*, *14*).

Over the course of the pH titration, there were marked ^1H and ^{15}N chemical shift changes for residues in the vicinity of H187, residues 184−198, in particular, N186, H187, T188, T192, K194, and E196 (which are at the C-terminus of helix II and in the following loop), and also in the C-terminus of helix I, where H155 resides (residues 154−159, in particular, H155, R156, and N159) (Figure 1B,C). These histidines are spatially close and partially buried in the folded structure of human PrP^C (Figure 1C) and are predicted by MD simulations to have pK_a values between 4 and 5 (*21*), significantly lower than the typical pK_a (≈6.6) for solvent-exposed histidine. The NMR chemical shift data suggest that these residues are indeed becoming protonated as the pH is reduced between pH 5.5 and 3.9, inducing some degree of conformational change in these regions of the protein. Direct observation of the protonation state of the analogous histidine (H186) in mouse PrP supports this as it is also partially deprotonated at pH 5.5 but becomes fully protonated at pH 3.5 (*23*).

In contrast, much smaller chemical shift changes are observed for residues surrounding the other histidine residues in the α-PrP

structured domain, namely, H140 and H177, showing that their ionization does not affect the local protein environment (Figure 1B,C). Both H140 and H177 are solvent-exposed in the NMR structures of human PrP at both pH 4.5 and 7.0 (*22*), with H177 fully protonated at pH 5.5 in mouse PrP (*23*). The lack of chemical shift change for these is consistent with computational data suggesting that these histidines are the least acidic in the structured region of human PrP, with pK_a values close to 7.0 (*21*). There are slightly larger chemical shift changes surrounding H140 (up to 0.1 ppm for ^{1}H and up to 1.0 ppm for ^{15}N), consistent with it being partially protonated at pH 5.5 (*23*), for example, in residues 141−144 (Figure 1B), but overall these are smaller and consistent with minor changes in hydrogen bonding patterns that do not affect the predominantly unstructured conformation of this region (*21*). Also of note are the small chemical shift changes at the C-terminus of helix III (residues 224−229), which are remote from any obvious titratable groups (*40*).

Structural Characterization of the PrP H187R Mutant. (*i*) *Solubility as a Function of pH*. To test the importance of the protonation state of histidine 187 in the native structure of PrP, we mutated this residue to arginine, thus imposing a permanent positive charge at this position in the protein. This mutant behaved in a manner radically different from that of wild-type α-PrP and would not refold in a soluble form at neutral or near-neutral pH values. It was possible, however, to refold the H187R mutant protein by dialysis under acidic conditions (pH < 4), and at these pHs, the protein was soluble over a wide range of concentrations. The refolded protein remained very sensitive to pH, aggregating rapidly at pH >4 (Figure 2A).

(*ii*) *Circular Dichroism*. We investigated the secondary and tertiary structure of wild-type and H187R mutant PrPs using CD spectroscopy (Figure 2B,C). The spectrum of wild-type PrP in its nativelike α-PrP conformation displays two minima at 208 and 222 nm, indicative of high α-helical content (Figure 2B). In contrast, the spectrum of H187R displays a single minimum at 215 nm (Figure 2B), characteristic of a high proportion of β-sheet, and is similar to that observed for wild-type PrP in its disulfide-reduced β-PrP conformation (*14*). This form of PrP is rich in β-sheet structure and displays many of the characteristics of a PrP^{Sc}-like precursor molecule, such as partial resistance to PK digestion, and the ability to form amyloid fibrils in the presence of physiological concentrations of salts (*14*). The aromatic CD spectra of H187R, α-PrP, and β-PrP (Figure 2C) also indicate a structural organization for H187R between that of α-PrP and that of β-PrP. H187R does not show the strong signal with a minimum at 272 nm given by α-PrP but retains a signal stronger than that of β-PrP or denatured α-PrP, with the minimum shifted to 280 nm. This is suggestive of an increase in residue asymmetry in the region of tryptophan at position 99 and an overall greater level of tertiary organization maintained in the H187R mutant compared with the β-PrP conformation.

(*iii*) *FTIR*. We further probed the secondary structure of H187R, α-PrP, and β-PrP by attenuated total reflection (ATR) Fourier transform infrared spectroscopy (see Figure 2D). The spectra cover the amide I absorption region, which is dominated by carbonyl stretching vibrations of the backbone amides. For β-PrP, there is a strong maximum at 1622 cm^{-1}, shown to be characteristic of amyloid structure (and distinct from nativelike β-sheet structure) by Zandomeneghi and colleagues (*41*), while α-PrP displays a maximum at 1652 cm^{-1}, characteristic of helical structure (*42*). The FTIR spectrum of H187R appears to be intermediate between those of β-PrP and α-PrP, suggesting both more β-sheet structure than α-PrP (signal at 1622 cm^{-1}) and more helical content than β-PrP (signal at 1652 cm^{-1}).

(*iv*) *Thioflavin T Binding Assay*. The nature of the H187R β-sheet structure was further probed through the binding of the benzothiazole dye, thioflavin T (ThT). ThT binding to a variety of amyloid fibrils causes a characteristic fluorescent spectrum alteration that does not occur on binding to precursor monomers or to amorphous aggregates of the polypeptide (*43*). ThT binding has been used frequently to follow the formation of prion amyloid fibrils in vitro (*44*, *45*) and as a diagnostic tool for the detection of infectious prions in brain tissue (*46*). Binding of ThT to H187R shows a significant increase in fluorescence in comparison to that of α-PrP (Figure 2E), indicating the presence of amyloid fibril structure in the H187R sample and confirming the characteristic "amyloid" signal at 1622 cm^{-1} observed in the H187R FTIR spectrum.

(*v*) *Sedimentation Velocity Analytical Ultracentrifugation*. Significant β-sheet content and a reduced level of tertiary structure for the H187R mutant are also features of β-PrP, which is predominantly oligomerized under native conditions (*14*). Thus, we studied the oligomerization state of wild-type α- and β-PrP and H187R using sedimentation velocity analytical ultracentrifugation (Figure 3A). We found that α-PrP sediments as a single species with a sedimentation coefficient of 1.73 S (Figure 3A). The data fitted with a frictional ratio of 1.4, which represents a slightly elongated species consistent with a protein with a core structured region (residues 121−230) and an unstructured, flexible N-terminal tail of 30 residues. The derived molecular mass of the species is 15.7 kDa, in good agreement with the expected mass of monomeric α-PrP. In contrast, the sedimentation distribution of β-PrP shows not a single species but a broad distribution of species between 1 and ∼30 S (Figure 3A). The average frictional ratio fitted for the distribution was 3.2, indicating a predominance of elongated species, which are nevertheless soluble as they are retained in preparation of the β-PrP conformer after centrifugation at 150000*g* (see Experimental Procedures).

The H187R mutant gives a sedimentation coefficient distribution distinct from those of both α-PrP and β-PrP but has features of each (Figure 3A). The H187R distribution shows a range of species present from ∼1 to > 30 S and fits to an average frictional ratio of 1.9, indicating that the majority of species are both large and elongated oligomers. Unlike β-PrP, however, H187R also shows a discrete peak at 1.44 S, comprising 16% of the total sample, and representing a monomeric species. The molecular mass derived for this species is ∼18 kDa, greater than that obtained for the α-PrP monomer, because of the higher average frictional ratio (which was fitted to the broad distribution of species).

(*vi*) *NMR Characterization of H187R*. The solubility of H187R at high concentrations allowed us to examine its properties using solution NMR. As shown previously, the NMR spectrum of α-PrP (Figure 3A,B) is characteristic of a fully folded globular protein, with wide chemical shift dispersion, including a number of resonances at frequencies of < 0.7 ppm (Figure 3A), which are indicative of strong tertiary interactions between aliphatic groups and aromatic rings. In contrast, the NMR spectrum of H187R displays a markedly reduced level of chemical shift dispersion (Figure 3A,B), indicating that the specificity of tertiary interactions characteristic of a fully folded protein is lost, consistent with the marked loss of an aromatic

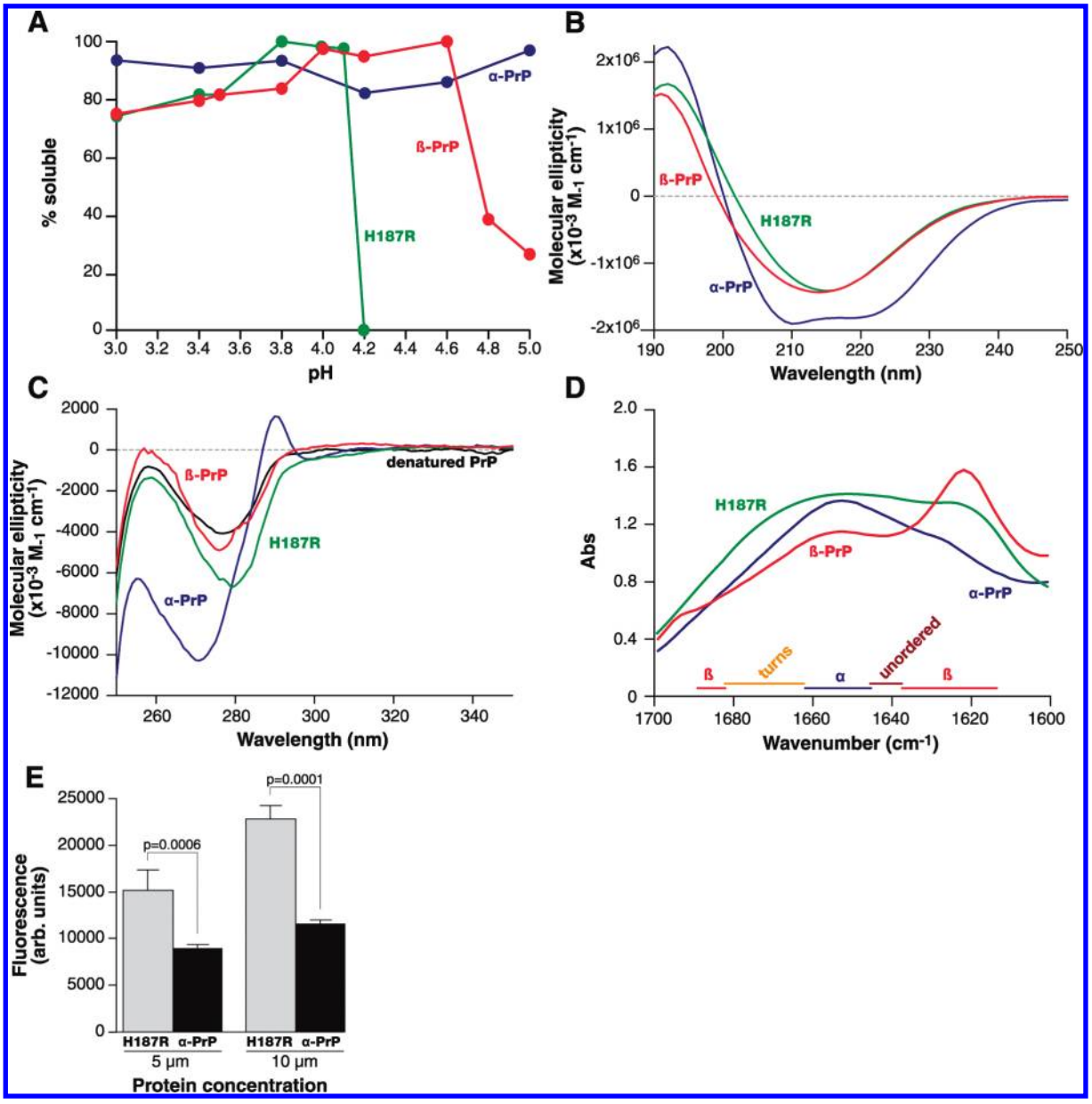

FIGURE 2: Physical properties of H187R, β-PrP, and native wild-type α-PrP. (A) Solubility of H187R, β-PrP, and α-PrP at various pHs. H187R shows a clear sensitivity to the solution pH, with an abrupt aggregation at pH >4.0. β-PrP is similarly sensitive, but to a lesser extent, while α-PrP is tolerant of a wide range of solution pHs. (B) Far-UV CD spectra of H187R, β-PrP, and α-PrP. Both H187R and β-PrP exhibit a clear single minimum at 215 nm, characteristic of β-sheet structure, with little evidence of α-helicity. α-PrP, in contrast, exhibits a typically α-helical spectrum, with double minima at 208 and 222 nm. The CD spectra are averages of 10 spectra and were collected at 20 °C between 190 and 250 nm. (C) Near-UV CD spectra of H187R, β-PrP, α-PrP, and denatured α-PrP. Native α-PrP shows a strong near-UV CD response, characteristic of a natively folded protein containing a well-defined tertiary structure and aromatic side chains in asymmetric environments, while denatured α-PrP lacks any distinct tertiary interactions. Both β-PrP and H187R show an intermediate level of organization, consistent with a partly folded state. The CD spectra are averages of 10 spectra and were collected at 20 °C between 250 and 350 nm. (D) Amide I region solution FTIR spectra of H187R, β-PrP, and α-PrP. The FTIR spectrum of β-PrP shows a clear peak at 1622 cm^{-1}, characteristic of amyloid β-structure (*41*). The spectrum of H187R is intermediate between those of β-PrP and α-PrP. Regions of the spectrum characteristic of specific secondary structures are indicated by horizontal bars at the bottom of the figure. (E) Thioflavin (ThT) binding to H187R and α-PrP. Binding of the benzothiazole dye, thioflavin T (ThT), to H187R results in an increase in fluorescence in comparison to that of α-PrP, indicating the presence of amyloid fibril structure in the H187R sample, consistent with the peak at 1622 cm^{-1} seen by FTIR.

(near-UV) CD signal (Figure 2C). The spectrum is broadly similar to that of β-PrP; however, H187R retains a degree of extra chemical shift dispersion [e.g., ≈8.7 ppm (Figure 3C)], consistent with the greater level of tertiary structure maintained in the H187R mutant than in the β-PrP conformation (Figure 2C).

The markedly reduced level of NMR chemical shift dispersion (Figure 3A,B) and near-UV CD signal (Figure 3D) indicate lost tertiary structure; however, the nativelike secondary structure shown by far-UV CD is characteristic of partly folded molten globule folding states (*47*). The fluctuating nature of the side chains in these states results in the "smearing" or broadening of NMR chemical shifts, which, depending on the time scale of the molecular motions, can cause loss of NMR signals altogether (*47*). Indeed, the number of observable peaks in the 1D ^{1}H NMR spectrum of H187R was significantly fewer than expected if all the proton resonances were observable, indicating that there is a loss of signal through line broadening, given the population of the monomeric species within the sample (≈16%) (Figure 3A).

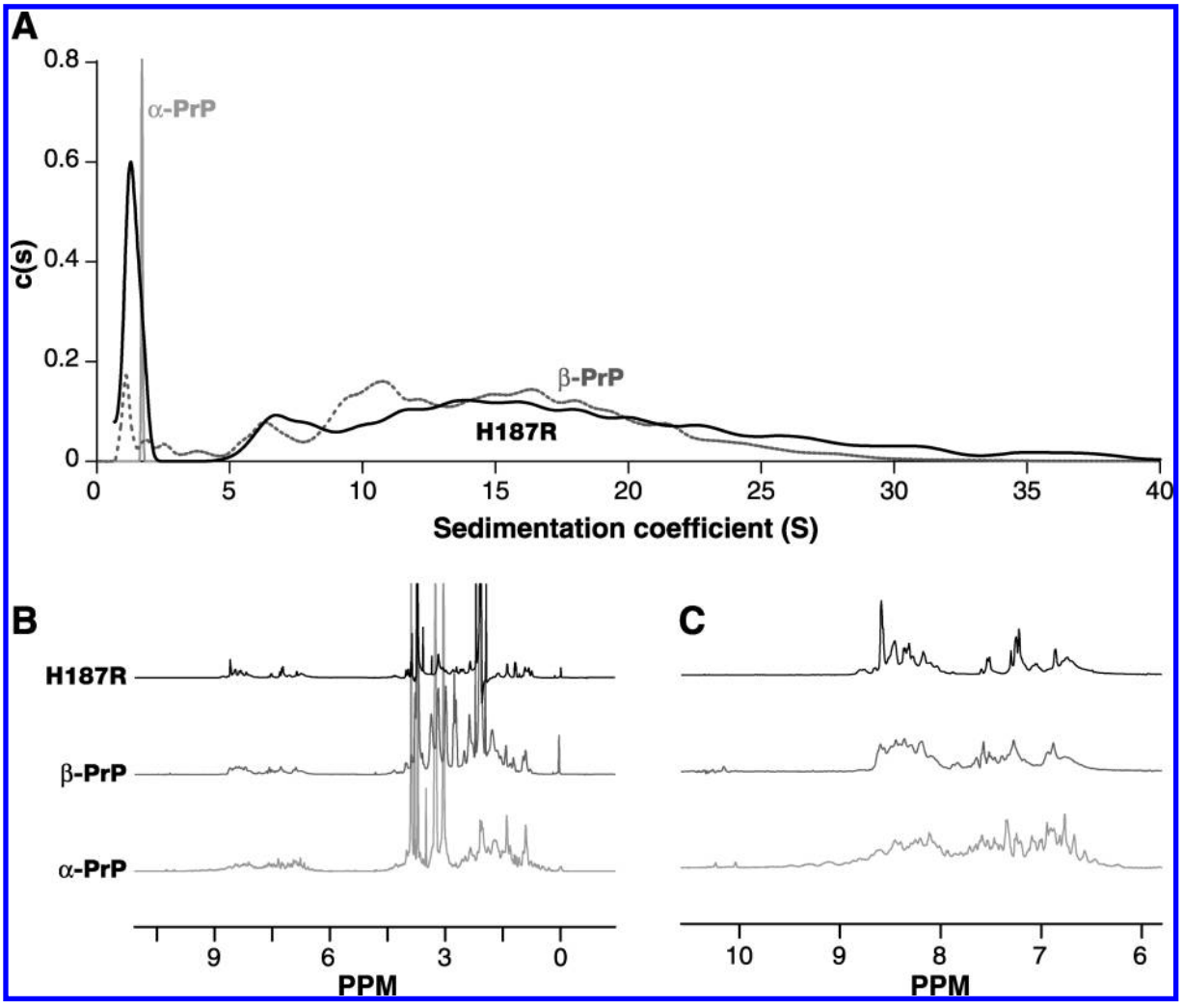

FIGURE 3: Oligomeric state and NMR spectra of H187R, β-PrP, and native wild-type α-PrP. (A) Sedimentation coefficient distributions derived from sedimentation velocity profiles for H187R, β-PrP, and α-PrP. A broad distribution of large species is present in both H187R and β-PrP samples, whereas α-PrP sediments as a discrete monomer at 1.7 S. (B and C) ^{1}H NMR spectra of H187R, β-PrP, and α-PrP. Full ^{1}H NMR spectra of H187R, α-PrP, and β-PrP (B) and expansion of the amide/aromatic region of the spectrum (5.8−10.5 ppm) (C). The spectra of both H187R and β-PrP exhibit a reduced level of chemical shift dispersion when compared to that of α-PrP, which exhibits resonances at a field higher than 0.7 ppm, characteristic of strong tertiary interactions between aliphatic groups and aromatic rings in this form of the protein. The loss of chemical shift dispersion is due to a markedly reduced level of tertiary structure, which is found in a number of partly folded "molten globule" folding intermediates. Despite the reduced level of shift dispersion, H187R and β-PrP exhibit markedly different spectra, indicating that they have different conformations.

Thus, given the oligomerization state of H187R (Figure 3A) and the loss of tertiary interactions (Figure 2B), it is likely that that the line broadening seen in the NMR spectra of H187R (Figure 3B) is due to a combination of conformational fluctuations on an intermediate (approximately millisecond) time scale (*48*), and increased rotational correlation time caused by the increased molecular mass of the oligomers. The majority of the observable NMR signals in H187R are likely to be from the unstructured N-terminus (residues 91−126), as these residues have chemical shifts very similar to those observed in the unstructured N-terminus of α-PrP, and also can be observed in β-PrP and a number of other partially folded intermediate states (*13*, *49*). There remains a possibility that resonances from other regions of the protein are visible, as the NMR spectra of H187R and β-PrP are radically different (Figure 3B), and there are also large differences in their solution characteristics. It is, however, not possible to differentiate signals arising from the monomeric and oligomer species.

(*vii*) *Protease Sensitivity of H187R.* Given the similarities between H187R and β-PrP in secondary structure and oligomerization state, we wished to compare the relative proteinase K resistance of H187R and α-PrP (Figure 4A). As with native PrP^C, α-PrP was extremely sensitive to PK digestion and was completely digested by the addition of 1 μg/mL proteinase K after 1 h. In contrast, H187R, like β-PrP (*14*), exhibited significant protease resistance, with visible cleavage products at PK concentrations of 100 μg/mL; its relatively high protease resistance likely to be caused in part by its predominantly oligomerized state.

(*viii*) *Determination of Disulfide Bond Status*. The presence of the disulfide bond linking helices II and III in PrP (residues 179 and 214) is crucial to its folding (*14*, *29*, *50*, *51*). Reduction of the disulfide bond, followed by refolding at acidic pH, results in the formation of β-PrP (*14*), which is highly amyloidogenic. PrP may also form amyloid fibrils under partially denaturing conditions with the disulfide bond intact (*12*, *18*, *52*). Given the proximity of the H187R mutation to the PrP disulfide bond, it is important to determine the status of the cysteine residues within the H187R mutant.

Following denaturation of the protein in GuHCl, an Ellman test for reduced cysteine residues (*35*) showed that the H187R

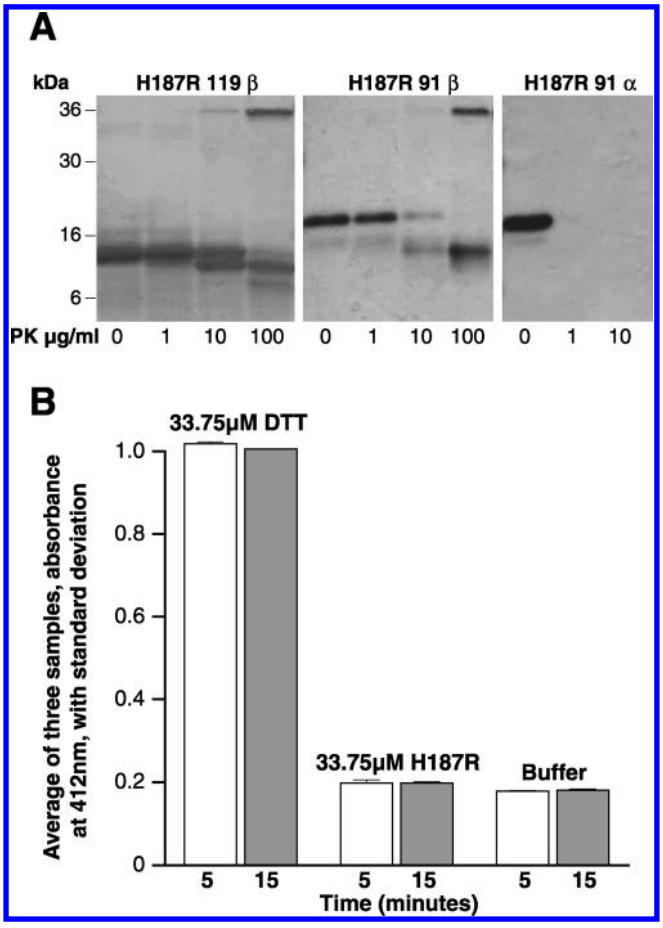

FIGURE 4: Cysteine oxidation status and protease resistance of H187R. (A) Protease K resistance and cleavage patterns of H187R and α-PrP. Protein samples were incubated with varying concentrations of proteinase K (0−100 μg/mL) in buffer at pH 3.5 and then analyzed by SDS−PAGE. H187R exhibited partial resistance to digestion with PK, whereas α-PrP is completely digested by PK at 1 μg/mL. (B) Determination of H187R cysteine oxidation [by the Ellman test (*35*)]. H187R contains no more reduced cysteines than the reference buffer sample, indicating that the cysteines are fully oxidized.

mutant contained no more reduced cysteines than the reference buffer sample (Figure 4B). We can thus conclude that the cysteines are fully oxidized; however, this does not show whether the disulfide remains intramolecular or is intermolecular, as found in the domain-swapped dimer of PrP (*50*). To resolve this, the H187R mutant was denatured by GuHCl under oxidizing and reducing conditions and analyzed using SDS−PAGE. Little increase in the intensity and/or number of high-molecular mass species was observed in the nonreduced sample, indicating the absence of intermolecular disulfide bonds in freshly prepared samples (data not shown).

DISCUSSION

Within the context of the protein-only hypothesis, it is proposed that mutations act by decreasing the thermodynamic stability of PrP^C, thus favoring the conversion to PrP^{Sc} through the increased concentration of the unfolded state and partially folded states (*1*, *53*). However, the effect of individual pathogenic mutations on the stability of PrP^C is variable, with no strong correlation between stability or structural perturbation of PrP^C and disease association (*9*). The precise relationship between mutation-induced perturbations of the PrP^C native state and the molecular basis of inherited prion disease thus remains unclear.

In this study, we have examined the pH-dependent fold stability of recombinant prion protein in its native cellular conformation and shown that the pH-dependent folding of α-PrP is critically dependent on the protonation of two key histidine residues. NMR chemical shift changes identify these as His187 and His155. Imposition of a positive charge at residue 187 through replacement of a histidine with an arginine markedly destabilizes α-PrP, resulting in a molecule that displays radically different conformational characteristics and that readily aggregates to form protease-resistant β-sheet-rich oligomers.

NMR chemical shift and structural data indicate that the primary effects of acidification between pH 6.4 and 4.0 are mainly in the C-termini of helices I and II, with the remainder of the protein largely unaffected. The structural nature of these chemical shift changes can be inferred from the solution structures of native human α-PrP at pH 4.5 and 7.0 (*22*). Although they retain broadly a very similar structure, there are significant changes in those regions that experience the largest changes in chemical shift upon acidification. In particular, in the solution structure at pH 4.5, the end of helix I (residues 144−154) is shortened, and the C-terminus of helix II (residues 186−194), where H187 resides, is less well-defined (*22*), indicating some destabilization and fraying of helix II. A study of wild-type mouse PrP, and a number of human pathogenic mutations mapped onto it, also shows that the C-terminus of helix II is significantly disordered under acidic conditions (pH 3.5), while other parts of the protein remain essentially unaffected (*23*). MD simulations of the effect of acidic pH on PrP^C indicate that the driving force for this destabilization is a rearrangement of the salt bridge between a protonated H187 and E196 (*21*, *22*, *54*), which in turn perturbs the salt bridges between H155 and R156 stabilizing the C-terminus of helix I (*40*). Taken together, the structural and chemical shift data indicate that although there is no clearly distinct intermediate state formed at acidic pH (pH 4.0), there are some significant conformational changes associated with the protonation of His187 and His155, i.e., an acid-induced destabilization and fraying of the C-terminus of helix II (and to a lesser extent helix I), suggesting that the protonation state of these residues may have a critical role in the pH-induced conformational transition of human PrP^C.

Indeed, several lines of evidence point to the importance of helix II (in particular its C-terminus) in the α to β conversion. The C-terminus of helix II provides the hinge in a three-dimensional domain-swapped dimer of human PrP (*50*) (in which the C-terminus of helix II is partly converted to a short β-strand) and appears to undergo a marked conformational change in ovine PrP^{Sc} (*55*). In β-PrP, which shows many of the attributes of a PrP^{Sc} precursor-like molecule, helix II also shows little α-helicity, unlike helices I and III (*14*). Helix II has also been identified as a potent initiator of the fibrillization of full-length mouse PrP, unlike the other major structural elements of PrP^C, and has been proposed to be the critical region for amyloid fibril formation in mouse PrP^C (*56*).

These observations are consistent with data that show that residues at the C-terminus of helix II, clustered around H187 and T188, have high conformational flexibility and are capable of undergoing a transition from an α-helical conformation to a β and/or random coil state (*40*). This region contains many so-called "α/β discordant" residues, which have been proposed to be associated with amyloid formation (*57*). These are residues that are normally found within β-strands but are present within α-helices in α-PrP (*57*); for example, the sequence TTTT (residues

190−193), at the end of helix II, is overwhelmingly found in β-strand or loop conformations within the Protein Data Bank (*40*). Indeed, the higher level of helix propensity in nonmammalian PrPs has been proposed to explain the reduced likelihood of them undergoing an $\alpha \rightarrow \beta$ conformational transition (*40*, *58*).

Although it is generally accepted that the conformational transition of PrP^C to PrP^{Sc} involves a shift from a predominantly α-helical conformation to one dominated by β-sheet structure, the regions of PrP involved in this conversion remain unclear. In particular, the extent and contribution of the α-helical C-terminal part of PrP^C in PrP^{Sc} β-sheet formation remain ambiguous. Models proposed for the structure of PrP^{Sc} include those in which helices II and III retain their native α-helicity (*59*, *60*). These contrast with data that show a redacted recombinant PrP lacking helix I (residues 23−88 and 141−176) retains the ability to support PrP^{Sc} formation in transgenic mice and form β-sheet-rich aggregates in vitro, suggesting that the β-sheet core region of PrP^{Sc} includes the region spanning helices II and III. Also, EPR and hydrogen exchange measurements of human recombinant PrP fibrils indicate that the β-sheet core of PrP amyloid consists of a parallel and in-register β-sheet structure formed through a major refolding of the C-terminal region of PrP^C (residues ∼160−220), implying that helix II and a large part of helix III should take part in the conformational transition (*52*, *61*).

The data presented here suggest that the protonation state of H187 may play a critical role in the maintenance of the native α-helical conformation of a "frustrated β region" of PrP^C and may be crucial in initiating possible conformational changes to a disease-competent state. Indeed, the H187R mutation in humans has been shown to cause the autosomal dominant inherited prion disease GSS (*24*, *25*, *27*). It is notable that many of the pathogenic mutations that are associated with inherited prion disease (T183A, H187R, T188R/K/A, E196K, F198S, E200K, and D202N) are found within this region of the protein, and that many of these mutations also introduce positive charge (*8*, *26*).

Interestingly, the equivalent substitution in mouse PrP (H186R) results in a markedly destabilized yet soluble protein (*23*). It should be noted that the effects of pathogenic mutations can differ, depending on the protein background (*62*). For example, NMR data, susceptibility studies, and transgenic models have shown that sequence variations that alter the rigidity of the normally mobile loop of residues 170−174 in PrP^C affect the specificity of infection, and mutations that increase the rigidity of this loop induce a spontaneous neurodegenerative disease in transgenic mouse models (*63*−*66*).

In general, the pH-induced ^{15}N chemical shift changes show no great correlation with those observed upon global unfolding (*7*); thus, they are not caused by a native-state to unfolded-state transition. Instead, these pH-induced shift changes closely resemble those observed with GuHCl denaturation in advance of the major unfolding transition, with similarly large chemical shift changes around the C-termini of helices I and II (*7*). The free energy and *m* value changes associated with these conformational changes appear to be relatively small, as the observed chemical shift changes do not display any apparent sigmoidal behavior (data not shown). It thus appears that both acidification and chemical denaturation have actions prior to the major unfolding transition and that the conformational changes induced are not simply due to a two-state transition from the folded to unfolded state but rather may be affecting the population of an aggregation-competent state.

ACKNOWLEDGMENT

We are grateful to Ray Young for preparation of figures and to Dave Scott of the National Centre for Macromolecular Hydrodynamics, University of Nottingham (Nottingham, U.K.), for his help in the analysis of the analytical ultracentrifugation data.

REFERENCES

1. Prusiner, S. B. (1998) Prions. *Proc. Natl. Acad. Sci. U.S.A. 95*, 13363–13383.
2. Collinge, J. (2001) Prion diseases of humans and animals: Their causes and molecular basis. *Annu. Rev. Neurosci. 24*, 519–550.
3. Griffith, J. S. (1967) Self replication and scrapie. *Nature 215*, 1043–1044.
4. Prusiner, S. B. (1982) Novel proteinaceous infectious particles cause scrapie. *Science 216*, 136–144.
5. McKinley, M. P., Bolton, D. C., and Prusiner, S. B. (1983) A protease-resistant protein is a structural component of the scrapie prion. *Cell 35*, 57–62.
6. Kuwata, K., Kamatari, Y. O., Akasaka, K., and James, T. L. (2004) Slow Conformational Dynamics in the Hamster Prion Protein. *Biochemistry 43*, 4439–4446.
7. Hosszu, L. L. P., Wells, M. A., Jackson, G. S., Jones, S., Batchelor, M., Clarke, A. R., Craven, C. J., Waltho, J. P., and Collinge, J. (2005) Definable Equilibrium States in the Folding of Human Prion Protein. *Biochemistry 44*, 16649–16657.
8. Mead, S. (2006) Prion disease genetics. *Eur. J. Hum. Genet. 14*, 273–281.
9. Liemann, S., and Glockshuber, R. (1999) Influence of amino acid substitutions related to inherited human prion diseases on the thermodynamic stability of the cellular prion protein. *Biochemistry 38*, 3258–3267.
10. Hornemann, S., and Glockshuber, R. (1998) A scrapie-like unfolding intermediate of the prion protein domain PrP(121−231) induced by acidic pH. *Proc. Natl. Acad. Sci. U.S.A. 95*, 6010–6014.
11. Swietnicki, W., Morillas, M., Chen, S. G., Gambetti, P., and Surewicz, W. K. (2000) Aggregation and fibrillization of the recombinant human prion protein huPrP90−231. *Biochemistry 39*, 424–431.
12. Baskakov, I. V., Legname, G., Baldwin, M. A., Prusiner, S. B., and Cohen, F. E. (2002) Pathway complexity of prion protein assembly into amyloid. *J. Biol. Chem. 277*, 21140–21148.
13. Gerber, R., Tahiri-Alaoui, A., Hore, P. J., and James, W. (2008) Conformational pH dependence of intermediate states during oligomerization of the human prion protein. *Protein Sci. 17*, 537–544.
14. Hosszu, L. L. P., Trevitt, C. R., Jones, S., Batchelor, M., Scott, D. J., Jackson, G. S., Collinge, J., Waltho, J. P., and Clarke, A. R. (2009) Conformational properties of β-PrP. *J. Biol. Chem. 284*, 21981–21990.
15. Arnold, J. E., Tipler, C., Laszlo, L., Hope, J., Landon, M., and Mayer, R. J. (1995) The abnormal isoform of the prion protein accumulates in late-endosome-like organelles in scrapie-infected mouse brain. *J. Pathol. 176*, 403–411.
16. Legname, G., Baskakov, I. V., Nguyen, H. O., Riesner, D., Cohen, F. E., DeArmond, S. J., and Prusiner, S. B. (2004) Synthetic mammalian prions. *Science 305*, 673–676.
17. Wang, F., Wang, X. H., Yuan, C. G., and Ma, J. Y. (2010) Generating a Prion with Bacterially Expressed Recombinant Prion Protein. *Science 327*, 1132–1135.
18. Makarava, N., Kovacs, G. G., Bocharova, O., Savtchenko, R., Alexeeva, I., Budka, H., Rohwer, R. G., and Baskakov, I. V. (2010) Recombinant prion protein induces a new transmissible prion disease in wild-type animals. *Acta Neuropathol. 119*, 177–187.
19. Kim, J. I., Cali, I., Surewicz, K., Kong, Q. Z., Raymond, G. J., Atarashi, R., Race, B., Qing, L. T., Gambetti, P., Caughey, B., and Surewicz, W. K. (2010) Mammalian Prions Generated from Bacterially Expressed Prion Protein in the Absence of Any Mammalian Cofactors. *J. Biol. Chem. 285*, 14083–14087.
20. Alonso, D. O. V., DeArmond, S. J., Cohen, F. E., and Daggett, V. (2001) Mapping the early steps in the pH-induced conformational conversion of the prion protein. *Proc. Natl. Acad. Sci. U.S.A. 98*, 2985–2989.
21. Langella, E., Improta, R., Crescenzi, O., and Barone, V. (2006) Assessing the acid-base and conformational properties of histidine residues in human prion protein (125−228) by means of pK_a calculations and molecular dynamics simulations. *Proteins 64*, 167–177.
22. Calzolai, L., and Zahn, R. (2003) Influence of pH on NMR structure and stability of the human prion protein globular domain. *J. Biol. Chem. 278*, 35592–35596.

23. Bae, S. H., Legname, G., Serban, A., Prusiner, S. B., Wright, P. E., and Dyson, H. J. (2009) Prion proteins with pathogenic and protective mutations show similar structure and dynamics. *Biochemistry 48*, 8120–8128.
24. Cervenáková, L., Buetefisch, C., Lee, H. S., Taller, I., Stone, G., Gibbs, C. J., Jr., Brown, P., Hallett, M., and Goldfarb, L. G. (1999) Novel *PRNP* sequence variant associated with familial encephalopathy. *Am. J. Med. Genet. 88*, 653–656.
25. Butefisch, C. M., Gambetti, P., Cervenakova, L., Park, K. Y., Hallett, M., and Goldfarb, L. G. (2000) Inherited prion encephalopathy associated with the novel PRNP H187R mutation: A clinical study. *Neurology 55*, 517–522.
26. Roeber, S., Grasbon-Frodl, E. M., Windl, O., Krebs, B., Xiang, W., Vollmert, C., Illig, T., Schroter, A., Arzberger, T., Weber, P., Zerr, I., and Kretzschmar, H. A. (2008) Evidence for a pathogenic role of different mutations at codon 188 of PRNP. *PLoS One 3*, e2147.
27. Hall, D. A., Leehey, M. A., Filley, C. M., Steinbart, E., Montine, T., Schellenberg, G. D., Bosque, P., Nixon, R., and Bird, T. (2005) PRNP H187R mutation associated with neuropsychiatric disorders in childhood and dementia. *Neurology 64*, 1304–1306.
28. Hosszu, L. L. P., Jackson, G. S., Trevitt, C., Jones, S., Batchelor, M., Bhelt, D., Prodromidou, K., Clarke, A. R., Waltho, J. P., and Collinge, J. (2004) The residue 129 polymorphism in human prion protein does not confer susceptibility to CJD by altering the structure or global stability of PrP^{C}. *J. Biol. Chem. 279*, 28515–28521.
29. Hosszu, L. L. P., Baxter, N. J., Jackson, G. S., Power, A., Clarke, A. R., Waltho, J. P., Craven, C. J., and Collinge, J. (1999) Structural mobility of the human prion protein probed by backbone hydrogen exchange. *Nat. Struct. Biol. 6*, 740–743.
30. Johnson, C. M., and Fersht, A. R. (1995) Protein stability as a function of denaturant concentration: Their thermal stability of barnase in the presence of urea. *Biochemistry 34*, 6795–6804.
31. Parker, M. J., Spencer, J., and Clarke, A. R. (1995) An integrated kinetic analysis of intermediates and transition states in protein folding reactions. *J. Mol. Biol. 253*, 771–786.
32. Atkins, P., and de Paula, J. (2006) Physical Chemistry, W. H. Freeman, New York.
33. Bodenhausen, G., and Ruben, D. J. (1980) Natural Abundance N-15 NMR by Enhanced Heteronuclear Spectroscopy. *Chem. Phys. Lett. 69*, 185–189.
34. Schleucher, J., Schwendinger, M., Sattler, M., Schmidt, P., Schedletzky, O., Glaser, S. J., Sorensen, O. W., and Griesinger, C. (1994) A general enhancement scheme in heteronuclear multidimensional NMR employing pulsed field gradients. *J .Biomol. NMR 4*, 301–306.
35. Ellman, G. L. (1958) A colorimetric method for determining low concentrations of mercaptans. *Arch. Biochem. Biophys. 74*, 443–450.
36. Schuck, P. (2000) Size-distribution analysis of macromolecules by sedimentation velocity ultracentrifugation and Lamm equation modeling. *Biophys. J. 78*, 1606–1619.
37. Laue, T. M., Shah, B. D., Ridgeway, T. M., and Pelletier, S. L. (1992) in Analytical Ultracentrifugation in Biochemistry and Polymer Science (Harding, S. E., Horton, J. C., and Rowe, A. J., Eds.) pp 90−125, Royal Society of Chemistry, Cambridge, U.K.
38. Wuthrich, K., and Riek, R. (2001) Three-dimensional structures of prion proteins. *Adv. Protein Chem. 57*, 55–82.
39. Swietnicki, W., Petersen, R., Gambetti, P., and Surewicz, W. K. (1997) pH-dependent stability and conformation of the recombinant human prion protein PrP(90−231). *J. Biol. Chem. 272*, 27517–27520.
40. Dima, R. I., and Thirumalai, D. (2004) Probing the instabilities in the dynamics of helical fragments from mouse PrPC. *Proc. Natl. Acad. Sci. U.S.A. 101*, 15335–15340.
41. Zandomeneghi, G., Krebs, M. R., McCammon, M. G., and Fandrich, M. (2004) FTIR reveals structural differences between native β-sheet proteins and amyloid fibrils. *Protein Sci. 13*, 3314–3321.
42. Goormaghtigh, E., Cabiaux, V., and Ruysschaert, J. M. (1990) Secondary structure and dosage of soluble and membrane proteins by attenuated total reflection Fourier-transform infrared spectroscopy on hydrated films. *Eur. J. Biochem. 193*, 409–420.
43. LeVine, H., III (1999) Quantification of β-sheet amyloid fibril structures with thioflavin T. *Methods Enzymol. 309*, 274–284.
44. Baskakov, I. V. (2004) Autocatalytic conversion of recombinant prion proteins discplays a species barrier. *J. Biol. Chem. 279*, 7671–7677.
45. Bocharova, O. V., Breydo, L., Salnikov, V. V., and Baskakov, I. V. (2005) Copper(II) Inhibits in Vitro Conversion of Prion Protein into Amyloid Fibrils. *Biochemistry 44*, 6776–6787.
46. Colby, D. W., Zhang, Q., Wang, S., Groth, D., Legname, G., Riesner, D., and Prusiner, S. B. (2007) Prion detection by an amyloid seeding assay. *Proc. Natl. Acad. Sci. U.S.A. 104*, 20914–20919.
47. Redfield, C. (2004) NMR studies of partially folded molten-globule states. *Methods Mol. Biol. 278*, 233–254.
48. Homans, S. W. (1989) A Dictionary of Concepts in NMR, Oxford University Press, Oxford, U.K.
49. O'sullivan, D. B., Jones, C. E., Abdelraheim, S. R., Thompsett, A. R., Brazier, M. W., Toms, H., Brown, D. R., and Viles, J. H. (2007) NMR characterization of the pH 4 β intermediate of the prion protein: The N-terminal half of the protein remains unstructured and retains a high degree of flexibility. *Biochem. J. 401*, 533–540.
50. Knaus, K. J., Morillas, M., Swietnicki, W., Malone, M., Surewicz, W. K., and Yee, V. C. (2001) Crystal structure of the human prion protein reveals a mechanism for oligomerization. *Nat. Struct. Biol. 8*, 770–774.
51. Welker, E., Raymond, L. D., Scheraga, H. A., and Caughey, B. (2002) Intramolecular versus intermolecular disulfide bonds in prion proteins. *J. Biol. Chem. 277*, 33477–33481.
52. Cobb, N. J., Sonnichsen, F. D., McHaourab, H., and Surewicz, W. K. (2007) Molecular architecture of human prion protein amyloid: A parallel, in-register β-structure. *Proc. Natl. Acad. Sci. U.S.A. 104*, 18946–18951.
53. Collinge, J., and Wadsworth, J. D. (2006) in Basic Neurochemistry (Siegel, G., Albers, R. W., Brady, S., and Price, D., Eds.) pp 791−803, American Society for Neurochemistry, Windermere, FL.
54. DeMarco, M. L., and Daggett, V. (2007) Molecular Mechanism for Low pH Triggered Misfolding of the Human Prion Protein. *Biochemistry 46*, 3045–3054.
55. Fitzmaurice, T. J., Burke, D. F., Hopkins, L., Yang, S., Yu, S., Sy, M. S., Thackray, A. M., and Bujdoso, R. (2008) The stability and aggregation of ovine prion protein associated with classical and atypical scrapie correlates with the ease of unwinding of helix-2. *Biochem. J. 409*, 367–375.
56. Yamaguchi, K., Matsumoto, T., and Kuwata, K. (2008) Critical region for amyloid fibril formation of mouse prion protein: Unusual amyloidogenic properties of the helix 2 peptide. *Biochemistry 47*, 13242–13251.
57. Paivio, A., Nordling, E., Kallberg, Y., Thyberg, J., and Johansson, J. (2004) Stabilization of discordant helices in amyloid fibril-forming proteins. *Protein Sci. 13*, 1251–1259.
58. Simonic, T., Duga, S., Strumbo, B., Asselta, R., Ceciliani, F., and Ronchi, S. (2000) cDNA cloning of turtle prion protein. *FEBS Lett. 469*, 33–38.
59. DeMarco, M. L., and Daggett, V. (2004) From conversion to aggregation: Protofibril formation of the prion protein. *Proc. Natl. Acad. Sci. U.S.A. 101*, 2293–2298.
60. Govaerts, C., Wille, H., Prusiner, S. B., and Cohen, F. E. (2004) Evidence for assembly of prions with left-handed β-helices into trimers. *Proc. Natl. Acad. Sci. U.S.A. 101*, 8342–8347.
61. Lu, X., Wintrode, P. L., and Surewicz, W. K. (2007) β-Sheet core of human prion protein amyloid fibrils as determined by hydrogen/deuterium exchange. *Proc. Natl. Acad. Sci. U.S.A. 104*, 1510–1515.
62. Hart, T., Hosszu, L. L. P., Trevitt, C. R., Jackson, G. S., Waltho, J. P., Collinge, J., and Clarke, A. R. (2009) Folding kinetics of the human prion protein probed by temperature jump. *Proc. Natl. Acad. Sci. U.S.A. 106*, 5651–5656.
63. Raymond, G. J., Bossers, A., Raymond, L. D., O'Rourke, K. I., McHolland, L. E., Bryant, P. K., III, Miller, M. W., Williams, E. S., Smits, M., and Caughey, B. (2000) Evidence of a molecular barrier limiting susceptibility of humans, cattle and sheep to chronic wasting disease. *EMBO J. 19*, 4425–4430.
64. Gorfe, A. A., and Caflisch, A. (2007) Ser170 controls the conformational multiplicity of the loop 166−175 in prion proteins: Implication for conversion and species barrier. *FASEB J. 21*, 3279–3287.
65. Meade-White, K., Race, B., Trifilo, M., Bossers, A., Favara, C., LaCasse, R., Miller, M., Williams, E., Oldstone, M., Race, R., and Chesebro, B. (2007) Resistance to chronic wasting disease (CWD) in transgenic mice expressing a naturally occurring allelic variant of deer prion protein. *J. Virol. 81*, 4533–4539.
66. Christen, B., Perez, D. R., Hornemann, S., and Wuthrich, K. (2008) NMR Structure of the Bank Vole Prion Protein at 20 °C Contains a Structured Loop of Residues 165−171. *J. Mol. Biol. 383*, 306–312.
67. Pettersen, E. F., Goddard, T. D., Huang, C. C., Couch, G. S., Greenblatt, D. M., Meng, E. C., and Ferrin, T. E. (2004) UCSF Chimera: A visualisation system for exploratory research and analysis. *J. Comput. Chem. 25*, 1605–1612.